Solar radiation effects on the Sardinia Radio Telescope performances

Alessandro Attoli, Sergio Poppi, Franco Buffa, Antonio Cazzani, Antonietta Fara, et al.

Alessandro Attoli, Sergio Poppi, Franco Buffa, Antonio Cazzani, Antonietta Fara, Davide Fierro, Francesco Gaudiomonte, Pasqualino Marongiu, Mauro Pili, Tonino Pisanu, Giannina Sanna, Giampaolo Serra, Flavio Stochino, Gian Paolo Vargiu, "Solar radiation effects on the Sardinia Radio Telescope performances," Proc. SPIE 12182, Ground-based and Airborne Telescopes IX, 1218203 (29 August 2022); doi: 10.1117/12.2628977

SPIE.

Event: SPIE Astronomical Telescopes + Instrumentation, 2022, Montréal, Québec, Canada

Solar radiation effects on the Sardinia Radio Telescope performances

Alessandro Attoli[a], Sergio Poppi[a], Franco Buffa[a], Antonio Cazzani[b], Antonietta Fara[a], Davide Fierro[c], Francesco Gaudiomonte[a], Pasqualino Marongiu[a], Mauro Pili[a], Tonino Pisanu[a], Giannina Sanna[b], Giampaolo Serra[d], Flavio Stochino[b], and Gian Paolo Vargiu[a]

[a]INAF–OAC Osservatorio Astronomico di Cagliari, Selargius, Italy
[b]DICAAR, Università degli Studi di Cagliari, Cagliari, Italy
[c]INAF-Sede Centrale, Roma, Italy
[d]Agenzia Spaziale Italiana (ASI), CSG-Unità Capo Sito Sardegna, Sede ASI-Cagliari, presso INAF–OAC Osservatorio Astronomico di Cagliari, Selargius, Italy

ABSTRACT

The Sardinia Radio Telescope, a 64-metre diameter fully steerable radio telescope operated by INAF, will be upgraded in order to extend its current operating frequency range 0.3-26.5 GHz up to 116 GHz, thanks to a National Operational Program (PON) funding assigned to INAF by the Italian Ministry of University and Research. The PON project is organized in nine Work Packages, one of which is dedicated to the accomplishment of a sophisticated metrology system designed to monitor the cause of the pointing errors and the reflector surface deformations. The entire antenna structure will therefore be equipped with a network of sensors, like thermal sensors, inclinometers, accelerometers, collimators, anemometers, strain gauges and others, to study environmental stresses and how they affect the SRT performances. This work is devoted to the investigation of the thermal stress effects produced by solar radiation. In particular, two analyses are carried out to confirm the relevance of a thorough temperature monitoring system, both conducted using Finite Element Analysis. First, a possible approach for the simulation of realistic thermal scenarios due to insolation is proposed and the effects on the pointing accuracy are analysed. Second, a feasible method to study the impacts that a differential heating of the Back Up Structure (BUS) produces on the radio telescope main reflector surface is presented. Finally, these effects are analysed as optical aberrations and modelled in terms of Zernike polynomials.

Keywords: Radio Telescope, Metrology System, Solar radiation, Pointing accuracy, Reflector surface errors, Optical aberrations, Finite Element Model.

1. INTRODUCTION

Inaugurated in 2013, the Sardinia Radio Telescope has just entered in its second development phase which will extend its current operating frequency range 0.3-26.6 GHz up to 116 GHz. This has been made possible thanks to a National Operational Program (PON) funding assigned to INAF by the Italian Ministry of University and Research to enhance scientific infrastructures operating in Southern Italy. The upgrade work plan is currently in progress and through nine work packages aims to achieve important targets including the purchase of new receivers and equipment for the development of microwave technology, the acquisition of High Performance Computing (HPC) systems and the implementation of a metrology system. The improved infrastructure will allow the scientific community to use SRT to explore the Universe at high radio frequencies, using the facility in both single dish and interferometric mode [1].
Receiving signals at high frequencies, up to 116 GHz as in this case, requires reliability, high antenna efficiency and the highest possible angular resolution. To achieve these goals, it is essential to study and characterise all those aspects that can downgrade the performances of the radio telescope by affecting the accuracy of the pointing and the antenna efficiency. Major causes of accuracy degradation in telescopes can be attributed to

Further author information: (Send correspondence to A. Attoli)
A. Attoli: E-mail: alessandro.attoli@inaf.it

Ground-based and Airborne Telescopes IX, edited by Heather K. Marshall, Jason Spyromilio, Tomonori Usuda,
Proc. of SPIE Vol. 12182, 1218203 · © 2022 SPIE · 0277-786X
doi: 10.1117/12.2628977

the effects of stresses produced by environmental loads on the facility structure. Particular attention must be given on gravitational action, which acts constantly with variable effects depending on the geometric profile of the antenna. But when high accuracy must be guaranteed, effects of thermal loads and wind force must be taken into account either.
If structural design according to homology principles [2] [3] [4] does not achieve the desired performances, active correction tools can be implemented in order to minimize errors. For example, the Sardinia Radio Telescope is equipped with active optics which consist of an active surface composed of panels that can be moved by actuators and a sub-reflector position control system.
This strategy becomes even more significant when mitigation of environmental effects is performed using metrological data. As mentioned above, one of the Working packages of the upgrade project consists in the development of a metrological system composed by a wide range of sensors. The sensors that will be placed on the telescope will belong to two main categories: the first will be responsible for characterising the magnitude of environmental actions, the second for explaining how the structure deforms as a result of the occurring stresses. Thermal sensors and anemometers belong to the first category, inclinometers, accelerometers, collimators and strain gauges to the second one.
In the dedicated scientific literature, many authors propose studies examining the influence of environmental loads on the structural behaviour of radio telescopes. For example, [5] studied the reduction of the TM65m pointing accuracy due to real temperature distributions acting on the alidade. The distortions generated by thermal loads were evaluated using inclinometers. Also [6] focuses on the alidade and evaluates the relationship between thermal loads and deformations suffered by the 32 meter VLBI parabola at Medicina. The experimental datasets were collected by placing thermal sensors in the alidade frame and an inclinometer in the elevation axis. [7] describes how inclinometers are used to monitor the impact of rail planarity on Sardinia Radio Telescope operation; in particular, the correlation between rail condition and temperature gradients is examined. The effects produced by the combined action of thermal load and wind force acting on ASTE 10-m Antenna are proposed in [8]. Certainly, the exponential increase in the computational power has encouraged numerical approaches to determine the response of complex structures to loads. For example [9] studies the effects on the pointing of a radio telescope caused by gravity, thermal loads and wind disturbances using a numerical approach based on the FE method. Another example of the use of FEM in radio astronomy infrastructure is proposed in [10], where the temperature dataset is applied to finite element models in order to calculate structural deformation of the IRAM 30-m submillimetric telescope. The approach illustrated in [11] provides for the use of photogrammetric surveys [12] as the only benchmark for updating the Finite Element model of the Sardinia RadioTelescope. This allowed to estimate with greater accuracy the displacements of the structure caused by gravity and thermal loads and to compare the results of the Finite Element analyses directly with the data deriving from the photogrammetric surveys [13].

After this brief introduction, a quick presentation of which environmental loads have to be taken into account during radio astronomical observations and which effects they produce on the antenna is given in Section 2. Section 3 is dedicated to the description of the correlation between solar irradiance and pointing error and numerical results of the Finite Element Analyses (FEA) are presented to explain the phenomenon. The errors on the main reflector surface generated by simplified but realistic thermal scenarios is presented in Section 4, where the optical effects are analysed in terms of the Zernike polynomial. Finally, concluding remarks and future developments are drawn in Section 5.

2. ENVIRONMENTAL LOAD

From the preliminary stages of design through to observation activities, it is essential to understand how environmental loads can influence the behaviour of a high precision instrument such as a radio telescope. Mostly, loads are due to gravity, wind or thermal stress.

Gravitational stress plays a crucial role, constraining the size of the antenna, the materials to be used and consequently the weight of the structure. Gravitational force is always present, but in a structure with numerous structural configurations, its effects change. [14]. In particular, in a steerable radio telescope that can change its elevation, gravitational action induces different stress conditions for each geometric configuration. Another aspect that must be considered is the possible presence of a lack of symmetry in the arrangement of the masses

in the structure, which can generate distorting phenomena in the elements of the alidade and rototranslations of the reflector. It is important not to ignore the action of the gravity force on the quadripod on which receivers and sub-reflector can be placed. At the same time, for each elevation angle, the effects of gravity are stationary and recur whenever the radio telescope is in that specific position. This makes it possible to determine the deformations induced for each elevation angle by means of formulations based on the finite element method (FEM) and, once they have been estimated, to act to compensate for the effects induced on the pointing and the main reflector surface. In particular, a parametric pointing model (PM) can be used to correct pointing errors and ,in case of radio telescopes equipped with active optics, like SRT, lookup tables (LUT) can be used to adjust the position of the second mirror with respect to the antenna optical axis, and even the surface deformation of the main reflector with respect the nominal shape by commanding electro-mechanical actuators.

The action of the gravitation loads is not the only cause of reflector surface accuracy loss, but also the environmental context in which the antenna is placed inevitably influences the telescope performances. The environmental stresses mentioned above have very different characteristics, particularly with respect to their variability and repeatability over time. For example, the magnitude of thermal loads and wind force vary randomly and cannot be considered repeatable as a function of antenna elevation angle. Another aspect to be taken into account is the load variation rate. This characteristic makes necessary to treat wind differently from temperature.

Analysing wind action is not easy. In fact, its variability in magnitude and direction can be instantaneous and the characterisation of its effects must include a dynamic study of the phenomenon. Generally, radio telescopes are designed with the Back Up Structure (BUS) rigid enough not to be deformed by wind under normal operating conditions. Normal operating conditions are specific to each radio telescope, and [15] describes those for SRT. However, the dish could act as a sail producing distortions in the alidade and misalignments in the quadripod. Several methods for modelling wind action are proposed in the literature; [16] proposes three approaches with different tools and techniques for acquiring and processing data. When the size of the antenna and the economic feasibility of the project allow it, radomes can be used, but these pose many problems in signal reception at short mm-wavelengths [2]. When the dimensions of the antennas are such as to discard solutions similar to those presented above, it is instead possible to identify operability thresholds, above which the radio telescope must suspend activity. Green Bank Telescope (GBT) adopts this strategy [17].

Thermal stress also belongs to the category of random and time-varying environmental actions. However, unlike wind, temperatures vary in structural elements with rate that allows them to be measured and their effects mitigated. This is because the elements have a specific thermal inertia depending on the material used in their construction. Studying the behaviour of antennas when subjected to thermal loads is very important, because differential expansion between elements can induce unexpected distortions and lead to pointing errors and surface errors that are not taken into account neither by the LUTs not by the pointing model (generally accomplished during nighttime). Protection against environmental temperature fluctuations can also be provided by radomes. Enclosing the entire antenna within an environment with a controlled climate by means of diffuse ventilation systems could represent a solution for the problems generated by thermal gradients [2].

To mitigate the effects on the surface of the reflector, a thermic shield is often installed to protect the BUS from environmental temperature changes, whether cooling or heating. A fan system can diffuse temperature-controlled air to keep the component at a uniform and constant temperature [4].

Certainly, a great support can be provided by the precise definition of the thermal condition of the telescope structural elements. This can be achieved by distributing thermal sensors in the most influential parts from a thermal point of view. The temperature dataset could also be used to perform finite element analysis (FEA) able to determine the deformations caused by a real field measured thermal scenario.

For the reasons described above and for the forthcoming implementation of a complex metrology system, this work has been devoted to the study of the thermal effects distributed on the structural body of the Sardinia Radio Telescope. The attention was focused on the phenomenon of overheating produced by the exposure to solar radiation, treating first the effects on the pointing, and then on of the main reflector.

3. SOLAR RADIATION EFFECTS ON SRT POINTING

In order to study the effects produced by solar radiation on the antenna pointing, first it is essential to define a parameter that allows univocal identification of the observing direction. For this reason, a vector originating at the intersection of the elevation axis and the azimuth axis (vertical axis) has been idealized. Under ideal conditions without any load on the structure, the vector points to the zenith when the elevation angle of the parabola is 90°, while it points to the horizon when the elevation angle is 0° (see, Fig. 1)

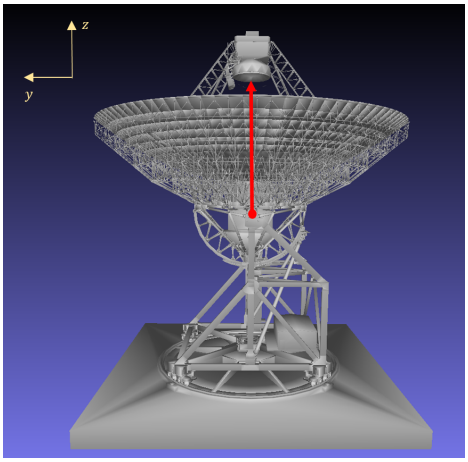

Figure 1. Pointing vector direction when the elevation angle is equal to 90°; the origin of the vector is located where the elevation axis intersects the azimuth axis, which under ideal conditions is perfectly vertical.

Therefore, in accordance with the direction in which the antenna receives the signal from the sky source, the direction of the vector changes as a function of the elevation and azimuth angles. It is important to remark that for the definition of the pointing vector, the presence of the sub-reflector has been neglected. This was possible because its alignment is ensured by moving mechanical actuators in accordance with the directions defined in a dedicated LUT. Due to the structural stresses produced by the external loads, the direction of the pointing vector and its position in space change with respect to the ideal condition. The distortions that occur in the structure generate translations and rotations in space of the pointing vector. However, since the observed sources are located at a distance that can be considered infinite, translation can be neglected. In order to understand how the structure behaves when thermally stressed and to identify the components that most influence the SRT's pointing when they are heated, a sensitivity analysis was performed using a finite element model. By iteratively applying a thermal load of 10°C to each of the 93.635 elements that make up the finite element model, the resulting vector rotation was estimated through the definition of the $PointingVectorRotation$ (PVR) parameter defined in Eq. 1

$$PVR = \sqrt{(\varphi_x)^2 + (\varphi_y)^2 + (\varphi_z)^2} \tag{1}$$

in which φ_x, φ_x and φ_x are the rotations around the Cartesian axes of the pointing vector with respect to the ideal direction. They should be zero in the ideal condition, while their values change as the pointing vector differs from the ideal position. By analysing the PVR value produced by the overheating of each of the elements, a ranking of the most important elements from a thermal point of view was made. Through a gradation of colour, Fig. 2 shows the rotation produced by each element, idealized with a point situated in its centre of gravity. Although Fig. 2 shows results of the sensitivity analysis for the 90° elevation only, studies at other elevation angles confirmed the results shown. The warmer colour tones indicate that the elements that generate greather pointing errors are located in the alidade. It is clear that thermal stress of the BUS and Quadrupod generates slight pointing vector rotations. The results are not surprising, as they confirm that the behaviour of the SRT model is coherent with the homology principles adopted in the design phase. Other important information emerged from this analysis is the elements of the structure where to install the thermal sensors. In this paper, only the results of the FEM analysis of the SRT alidada thermal behaviour under solar radiation heating will be presented. The alidade is the structural frame that supports all the moving components that can tilt around

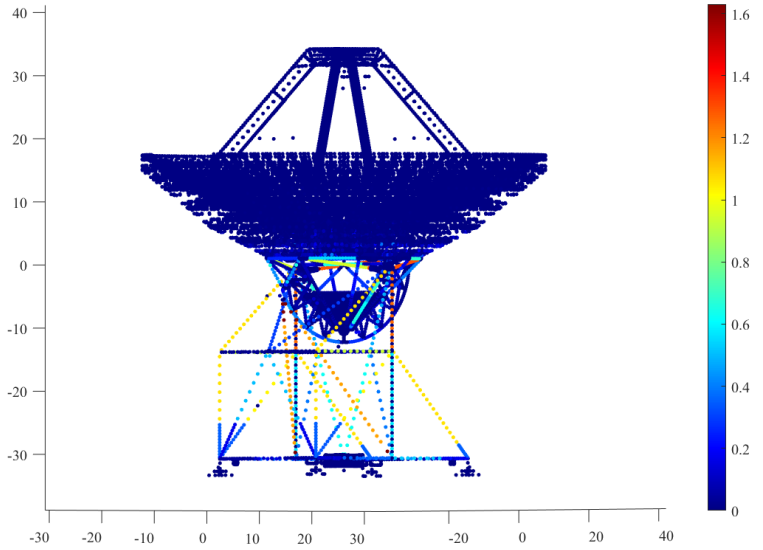

Figure 2. Map of the influence on the pointing of each element of the finite element model with elevation angle equal to 90°. The colour gradation of each point in the map represents the amount of PVR (expressed in arcsec) produced by the element it represents.

the elevation axis; it can rotate around the azimuth axis thanks to four movement systems with two bogies each. It is composed of 49 trusses. Studying solar radiation phenomena is not easy, especially when it is matter of analysing its effects on a complex structure such as a radio telescope. In fact, the exposure of each part to the sun's rays is linked to the position of the sun during the day, but also to the azimuthal orientation of the antenna and the angle of elevation at which the radio telescope is operating [18]. In fact, the shading produced by the dish on the structural elements of the alidade and the inverted umbrella-cradle system can play an important role in the behaviour of the antenna. The commercial Autodesk Revit software [19] was used to estimate the solar radiation that reaches each truss of SRT considering shadows and reflections generated by the other radio telescope components. The incident solar radiation I_i is evaluated through Eq. 2

$$I_i = (I_b \ \cos\vartheta \ F_{sh}) + (I_d \ F_{sk}) + I_g \tag{2}$$

where I_b is the direct beam radiation which is measured perpendicular to the sun, ϑ is the incident angle of the radiation on the surface, F_{sh} represents the fraction of the surface overshadowed by the close antenna elements, I_d is the diffuse sky radiation, F_{sk} is the fraction of the diffuse sky visible in this instant from the surface and I_g is the radiation reflected from the ground.
The software includes a database of local climatic data, that allows to obtain a hourly profile of environmental temperatures, i.e. an essential information in the proposed analytical model. In order to estimate the radiation incident on each truss, the average value of the radiation striking the four faces of the three-dimensional truss was calculated. It was therefore possible to obtain the total radiation that hits each truss at each hour of the day. This parameter is indispensable for the calculation of the structural element temperature due to its exposure to the sun's rays. With the aim to estimate the temperature reached by each element, the following has been assumed:

- Trusses are considered opaque bodies, so they do not transmit energy, but are only able to reflect and absorb it.
- In the evaluation of the heat exchange, the effect of conduction between the various elements in contact with each other was neglected; the temperature is due exclusively to radiation and convection. Although the model appears simplified, analyses have shown that the effect of conduction between two trusses extends

for a distance from the contact point that is irrelevant to the length of each truss; therefore, it does not contribute as much in estimating the average element temperature.

- The time span considered corresponds to one hour; this interval allows stationary conditions to be considered.

Based on these assumptions, the value of the exchanged energy can be described through the energy balance in control volume expressed in Eq. 3 [20] [18]:

$$G = \rho G + h_c \ (T_p - T_a) + \varepsilon\sigma \ T_p^4 \tag{3}$$

In which ρ is the reflection coefficient of a surface, G is the solar radiation that strikes the same surface, h_c is the convection coefficient between the surface and the air, T_p is the surface temperature, T_a is the environmental temperature, ε is the emissivity and σ is the Stefan-Boltzmann constant (4)

$$\sigma = 5,67 \ 10^{-8} \ \ [\frac{W}{(m^2 \ K^4)}] \ . \tag{4}$$

The reflection coefficient ρ and the emissivity ε are expressed as a function of the surface conditions of the real body. For a white paint surface treatment as in the case of SRT the following values for emissivity and reflection coefficient can be respectively assumed : $\varepsilon = 0.88$, $\rho = 0.86$. Concerning the convection coefficient , if the fluid is not forced air h_c assumes values between 2.5 and 25 $W/(m^2K)$ [21] and in this case it is set equal to 20 $W/(m^2K)$. Once the solar radiation G and the environmental temperature T_a have been simulated by Autodesk Revit, T_p in Eq. 3 can be solved by a numeric method.
However, the analytical model needs to be calibrated so that the simulated temperatures are comparable with the real ones. The calibration is done by adjusting only a few of the parameters governing the energy balance, i.e. the reflection coefficient ρ and the emissivity ε, which are characteristic of the surface treatment of the materials. The ideal values of the coefficients will differ from the real ones. This is due to the state of the paint covering the structure, which shows imperfections due to normal weathering and oxidation typical of metal systems. The experimental dataset, on the other hand, was obtained by thermographic surveys carried out using a thermal imaging camera hosted in a drone. The investigations were carried out in the daytime hours of September,11_{th} 2020 , November, 19_{th} 2020 and December, 31_{th} 2020.
The images were captured on the four sides of the radio telescope in order to frame and characterise a number of trusses useful for validating the calculation model developed. In order to validate the temperatures measured with the thermal camera, a point measurement of the trusses was performed using an infrared thermometer. By calculating the average of the temperatures in the four faces of the trusses, it was possible to estimate a value closer to the real value; in addition, the temperature of each truss face was estimated as the average of the values measured at three points, i.e. at the centre and at both ends (Fig. 3). By applying a least squares approach comparing the temperatures measured on site, which are adopted as benchmark, and the temperatures simulated with the analytical model, the values of the emissivity ε and reflection coefficient ρ were obtained equal respectively to $\varepsilon = 0.65$ and $\rho = 0.60$.
With the aim of studying the Sardinia Radio Telescope's behavior in most of the possible solar exposure scenarios in which it may operate during the year, thirty-six simulations were performed. In particular, four representative days of each season of the year (February 5_{th}, May 5_{th}, August 5_{th} and November 5_{th}), falling in the middle of the respective season (Winter, Spring, Summer, Fall) were chosen; for each day nine configurations were analysed at three elevation angles (80°, 60° and 30°) and three orientation of the antenna in the North, East and South direction. The simulations were developed considering a reference local time (12:00) for all the cases under study. Thus, each set of simulated temperatures corresponding to a given scenario were applied to the finite element model for the calculation of the resulting antenna pointing error.

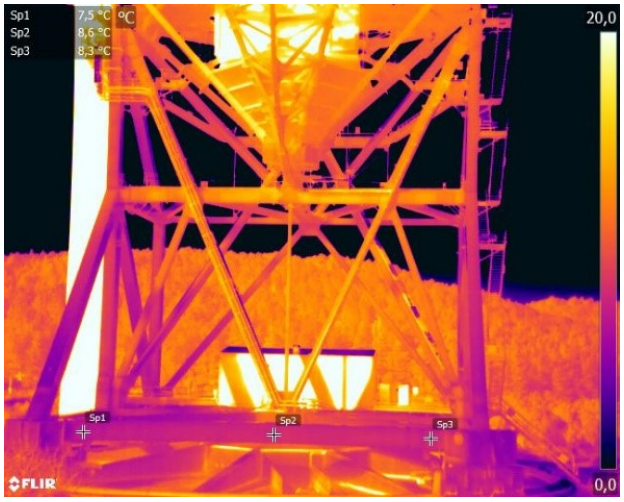

Figure 3. Example of the three truss points location in which the temperature were detected.

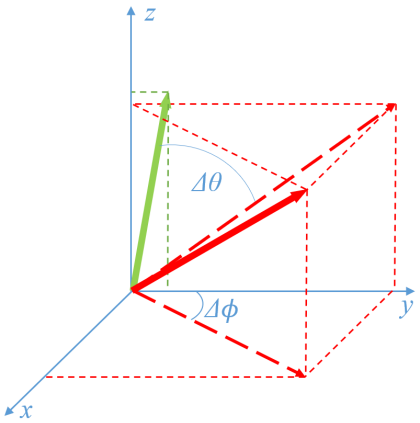

Figure 4. Representation of the final position of the pointing vector reached as a result of a hypothetical thermal scenario; in addition, the figure shows the generated angular errors in terms of elevation and azimuth angle variation.

In Fig. 4, the green vector is the pointing vector in the ideal non-deformed condition in the case where the elevation angle is equal to 80°. The red one is the pointing vector in the position reached as a result of the distortions produced by the thermal loads. The figure therefore shows how the rotations undergone by the pointing vector around the three Cartesian axes can be expressed in terms of elevation angle $\Delta\theta$ and azimuthal angle $\Delta\phi$ variations, i.e. the antenna degree of freedom (DOF). In Fig. 5 the histograms show the values of $\Delta\theta$ and $\Delta\phi$ produced by two of the thirty-six thermal scenarios analysed, considered representative. In particular, the first case presented refers to the condition with elevation angle equal to 80° and and exposed according to the east orientation; the second case refers to the condition with elevation angle equal to 30° and exposed according to the south orientation. Different colours were used for each representative day of the season.

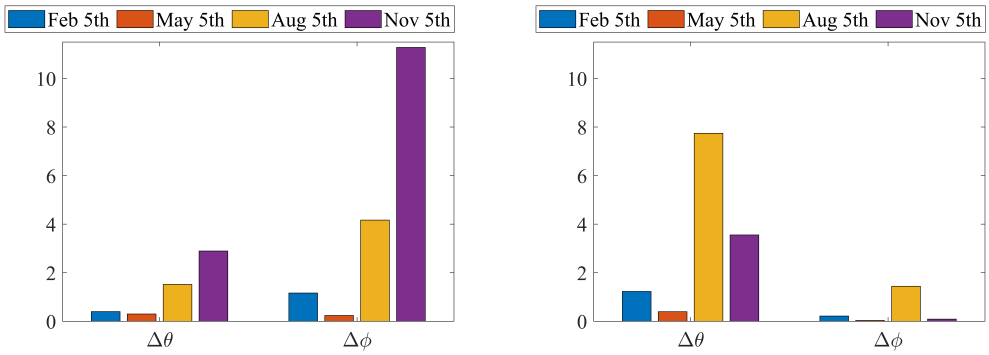

Figure 5. Elevation and azimuth angle variation (in arcsec) produced by solar radiation for two representative thermal scenarios. On the left are presented the results for simulations in which the antenna is positioned with elevation angle equal to 80° and exposed according to the east orientation; on the right are presented the results for simulations in which the antenna is positioned with elevation angle equal to 30° and exposed according to the south orientation.

The reduction in pointing accuracy shown in the diagrams proves that the structural behaviour of SRT is affected by the presence of thermal loads.

The results also show that increasing environmental temperature throughout the year does not inevitably produce a reduction in pointing accuracy. In fact, it can be seen in the histogram on the left of Fig. 5 that, in the specific scenario simulated, the variation of the elevation and azimuth angles in November is more than those detected in August, a month when environmental temperatures are significantly much higher. Thus, no seasonal trend was found in the obtained results. On the other hand, it can be seen that the influence of the temperature distribution in the 49 structural elements of the alidade is dominant. Furthermore, investigating the structural behaviour in more detail, it has been found that the magnitude of $\Delta\phi$ is linked to the temperature difference among the truss that are symmetrically located with respect to the plane of symmetry of the alidade. To make this more clear, purple-colored trusses in Fig. 6. produce opposite azimuth rotations. In particular, if their temperature is the same, their effects counterbalance each other; whereas, if they have different temperatures, azimuth rotations are generated. For example, in the leftmost graph of Fig. 5, it can be observed that at elevation 80°, with an eastern orientation, $\Delta\phi$ exceeds 11 arcsec in November and less than 5 arcsec in August. Comparing the two thermal scenarios, it was observed that there are greater temperature differences among the symmetrical trusses in the fall simulation than in the summer simulation.
On the other hand, the magnitude of $\Delta\theta$ depends on the temperature difference among the trusses, which, as they expand due to thermal loads, generate opposite rotations in elevation. Referring again to Fig. 6, thermal expansion of the green trusses produces an increase in elevation angle, while heating of the purple trussess generates a reduction in elevation angle. In the right graph of Fig. 5, it can be observed that at elevation 30° with a southern orientation, $\Delta\theta$ reaches almost 8 arcsec in August and 1 arcsec in February. In fact, the temperature differences among the trusses that generate opposite rotations in elevation are greater in the summer month simulation.
It is clear that all these aspects are inevitably linked to the different radiation of the structural elements caused by the geometric configuration in which the antenna is set during its operations.

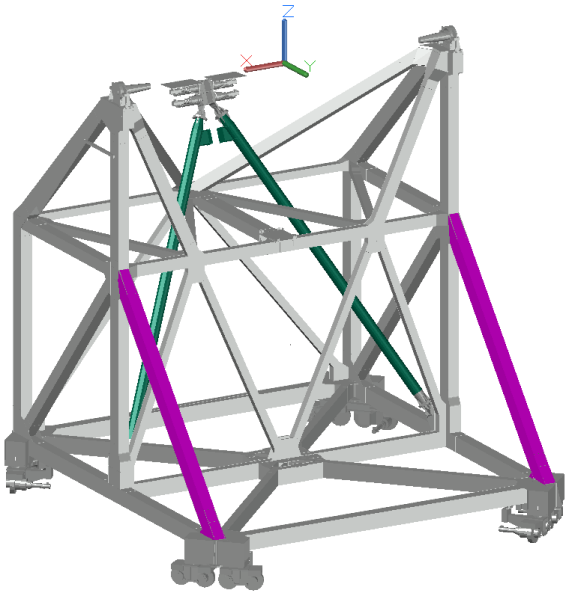

Figure 6. Structural arrangement of the alidade in which symmetry with respect to the y-z plane and lack of symmetry with respect to the x-z plane are shown. In addition, the image highlights some trusses that affect the antenna pointing in different ways.

4. SOLAR RADIATION EFFECTS ON SRT PRIMARY REFLECTOR SURFACE

This section is devoted to the study of the effects on the main mirror of the Sardinia Radio Telescope produced by the differential heating of the BUS elements due to solar radiation. The purpose is to investigate large-scale deformations on the surface of the primary reflector generated by distortions in the structural system that supports it [4]. The deviation from the best fit parabola generates a variation in the path length of the incoming wavefront on its way to the focal point, where the receivers are located. Thus, the arising phase errors distort the beam pattern and this results in a loss of aperture efficiency [22][23].
It is important to remark thatin the FEM model of the SRT main reflector surface here considered, the best surface alignemnt was set at 45°. This aspect will take on greater relevance later.
Simplified thermal scenarios, but representative of a realistic temperature distribution, were identified. Then, thermal simulations were implemented in the finite element model in order to determine the deflections detected on the surface of the reflector with respect to the ideal parabolic shape.

An ad-hoc MATLAB^{TM} script was used to determine the displacement undergone by each reflector panel along the orthogonal direction w.r.t. the related panel surface: the deviation from the best-fit paraboloid is then the surface error evaluated in the following.

At first, the 30°, 60° and 80° elevation configurations were analyzed, in which the entire BUS was stressed with a uniform thermal load of 5°C. The analyses were carried out including gravity to compare the effects of the two different loads. Fig. 7 shows the map of deflections achieved for a elevation angle equal to 30°, the first due only to the gravitational load (left), the latter due to the presence also of the uniform thermal load over the whole BUS (right).

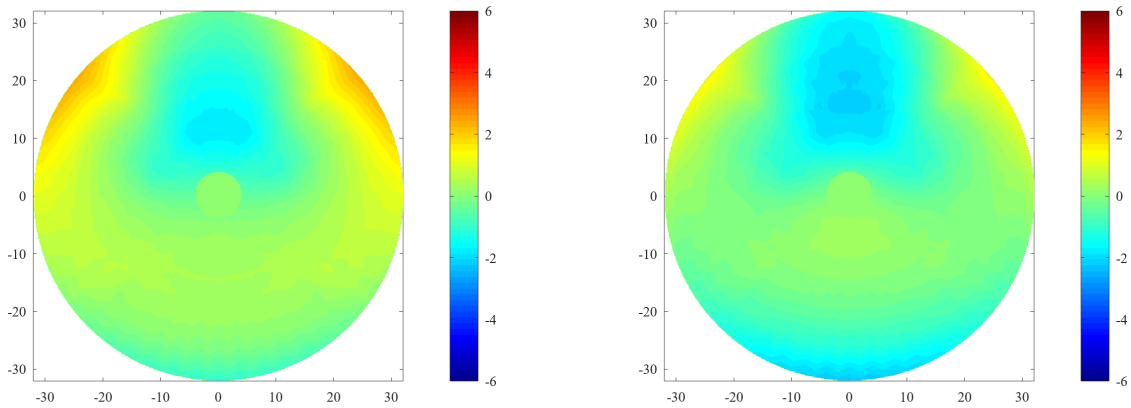

Figure 7. Maps of deflections estimated at 30° elevation angle. The left map refers to the case in which only gravitational load is applied; the right map refers to the case in which both gravitational and thermal loads are applied to the whole BUS. The abscissae and ordinates are expressed in metres, while the deflections are expressed in millimetres.

A quantitative evaluation of the surface accuracy loss due to heating of the BUS can be made by using the root mean square (RMS) value of the map deflections. Tab. 1 describes the estimated rms values produced by the SRT FEM simulation of the presented elevation and load conditions.

Table 1. Comparison between rms values [mm] of the main reflector surface accuracy calculated in three different FE scenarios (30°,60°,90°) when only gravitational load is applied on FE model (second row) and when both gravitational and a uniform thermal load of 5°C applied on the whole BUS stressed together the FE model (third row).

Elevation angle [deg]	30	60	80
Gravitational load rms [mm]	0.809	0.911	2.087
Gravitational and Thermal loads rms [mm]	0.770	0.998	2.150

By examining the rms values in Table 1 it can be seen that rms value produced by the gravitational effect increases as the elevation angle changes from 45°, elevation at which the best-fit parabola was set during the antenna construction. It is also clear that the deflections produced by gravity are predominant compared to the effects produced by thermal load. However, the magnitude of the displacements produced by thermal action should not be neglected and provide a contribution to the surface error of the main reflector (Figs.9 - 10).

For the elevation angle equal to 30°, the thermal action decreases the rms value; the opposite situation occurs in the two cases where the elevation angles are higher than 45°. Indeed, at elevations less than 45° the reflector deflections generated by the thermal load have opposite direction with respect to the deflections produced by the gravitational load.

In the case where only one side of the radio telescope is subject to solar exposure, non-negligible thermal gradients can develop between radiated and shaded parts. For example, if the radio telescope starts its activity after having been parked at the zenith with only one side exposed to the solar radiation. By properly analysing the thermal images produced in the survey campaign described in the previous section, it was possible to note that the irradiated portion of the BUS can reach temperatures 5°C higher than the shaded portion (see the leftmost image of Fig. 8).

Then, at the three elevations already considered, SRT FEM scenarios were analysed in which only half of the BUS was undergone to a thermal load of 5°C with respect to a reference temperature set in the Finite Element model: first the side with positive y, then the side with positive x (see the rightmost image of Fig. 8). The reference temperature defines the state from which thermal expansion or contraction starts. Again, the

contribution to loss of surface accuracy due to thermal action was compared with that produced by gravitational action.

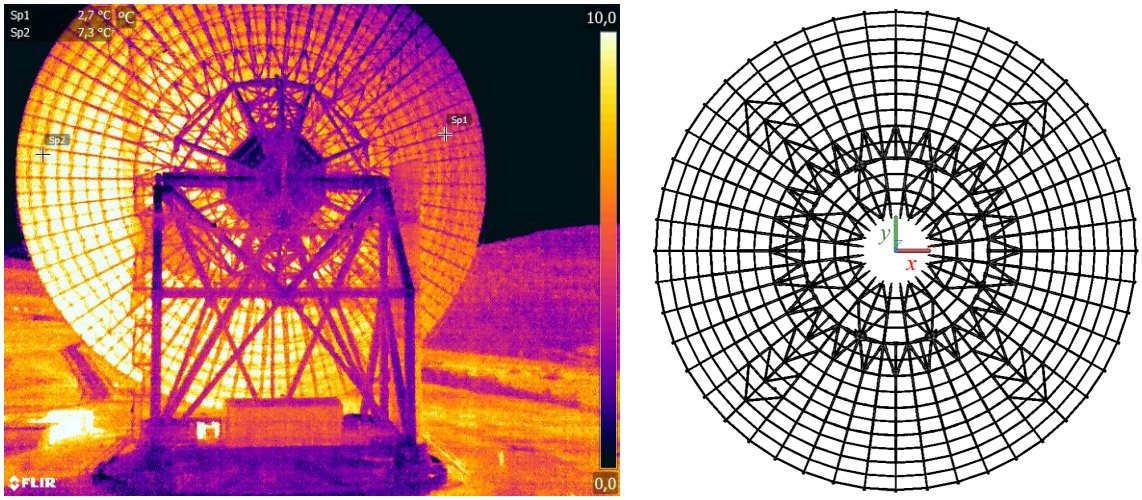

Figure 8. On the left: Thermographic survey performed with a thermal imaging camera housed in a drone: it can be detected: it can be observed the thermal gradient between the irradiated side of the BUS and the shaded side detected even at low elevation angles; on the right: identification of Cartesian axes adopted for temperature distribution in the load configurations.

Fig. 9 shows the deflection maps calculated considering two SRT FE scenarios at 80° elevation when only gravitational load are applied to the FE model (left panel) and then when to the gravitational load a 5°C thermal load has been added, but only on the elements in the right half of the BUS (right panel).

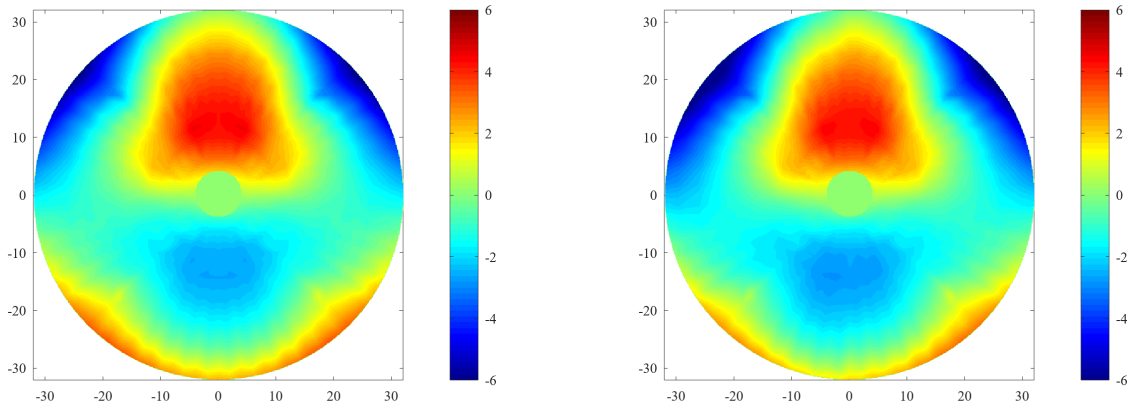

Figure 9. Maps of deflections detected at 80° elevation angle. The left map refers to the case in which only gravitational load is applied; the right map refers to the case in which to the gravitational load has been added a 5°C thermal load to the right half of the BUS (x_+ side). The abscissae and ordinates are expressed in metres, while the deflections are expressed in millimetres.

Fig. 10 on the other hand shows the deflection maps calculated considering two SRT FE scenarios at 60° elevation when only gravitational load are applied to the FE model (left panel) and then when to the gravitational load a 5°C thermal load has been added, but only on the elements in the upper half of the BUS (right panel).

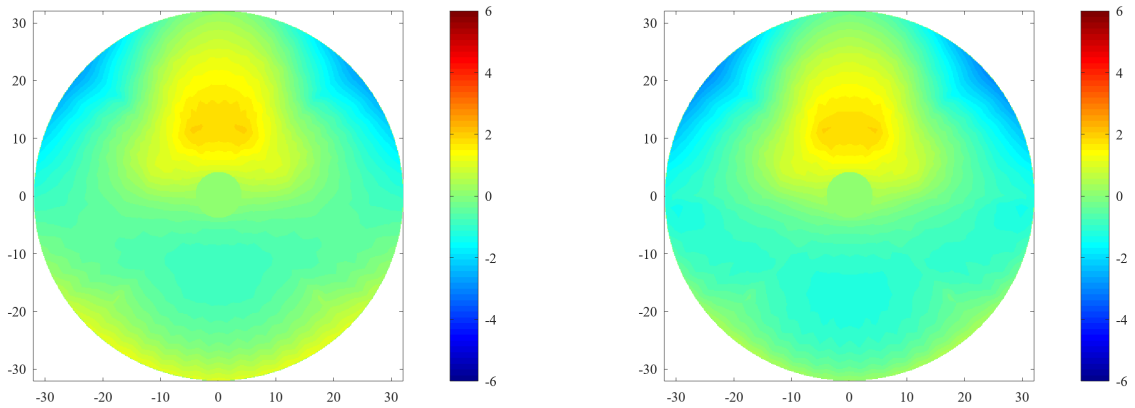

Figure 10. Maps of deflections detected at 60° elevation angle. The left map refers to the case in which only gravitational load is applied; the right map refers to the case in which to the gravitational load has been added a 5°C thermal load to the upper half of the BUS (y_+ side). The abscissae and ordinates are expressed in metres, while the deflections are expressed in millimetres.

Table 2. Comparison between rms values [mm] of the main reflector surface accuracy calculated in three different FE scenarios (30°,60°,90°) when to the gravitational load a 5°C thermal load has been added, but only on the elements in the upper half of the BUS (second row) and when to the gravitational load a 5°C thermal load has been added, but only on the elements in the right half of the BUS (third row).

Elevation angle [deg]	30	60	80
Upper half of the BUS (y_+ side) rms [mm]	0.809	0.911	2.087
Right half of the BUS (x_+ side) rms [mm]	0.772	0.949	2.123

Table 3. Variation in [%] of the rms parameter due to the action of both gravitational load and 5°C thermal load with respect of the rms generated by only the gravitational action.

Elevation angle [deg]	30	60	80
Whole BUS Δrms [%]	-5	16	4
Upper half of the BUS (y_+ side) Δrms [%]	0	5	1
Right half of the BUS (x_+ side) Δrms [%]	-5	10	3

Table 2 shows the rms values for all the cases described where the simultaneous action of gravity and a temperature gradient of 5°C between exposed and shaded side was considered. In the load scenarios simulated, the results reveal that for the elevation angles equal to 60° and 80°, the rms value is higher when the right half of the BUS is heated; on the other hand, for the 30° elevation angle, the rms value is higher when the upper half of the BUS is thermally stressed.

Moreover Table 3 shows the percentage variation of the rms parameter due to the action of both gravitational load and thermal load with respect to the rms generated by only the gravitational action, for all elevation and load combinations analyzed.

Interesting aspects arise by comparing the values of the rms values in Table 3. The influence of thermal action is greatest when the stress is acting on the whole BUS. Once again, the results reveal that, for the simulated load conditions, thermal stress reduces the rms value when the elevation angle is 30°. Besides, for elevations slightly higher than 45° (e.g., 60°), thermal action generates increases in rms value greater than 10 %; this occurs

because, for the same thermal effects, the deflections due to gravitational loading are lower.
It is worth to notice that, the radio telescopes equipped with active surface (as SRT) would be able to correct for such deformations, provided that a quasi real-time mapping of the main reflector surface were performed. Several authors propose to approach the study of the phenomenon by considering the total surface deformation as the superimposition of multiple optical aberrations.[4][22]. In fact, in the absence of such a facility it is interesting to understand how deformations of the reflector surface can affect the antenna optics.
For this reason, the deflection maps were modelled in terms of the Zernike polynomial [24]. The representation of the deformation maps by an orthogonal base of Zernike polynomials makes possible to distinguish what kind of optical aberrations affect the main reflector surface accuracy, when this latter undergoes to thermal and gravitational loads. Equation 5 is the analytic expression of the Zernike polynomial representation used here to represent the optical aberration related to the deformation maps, where $Z_j(x, y)$ are the polynomial components and W_j are the weights that quantifies the magnitude of each component [25]. In our case, 21 Zernike components were used to represent the deformation maps of the SRT reflector surface simulated by the FE model.

$$W(x, y) = \sum_{j=0}^{j_{max}} W_j Z_j(x, y) \tag{5}$$

where j_{max} is set equal to 21 in our case.

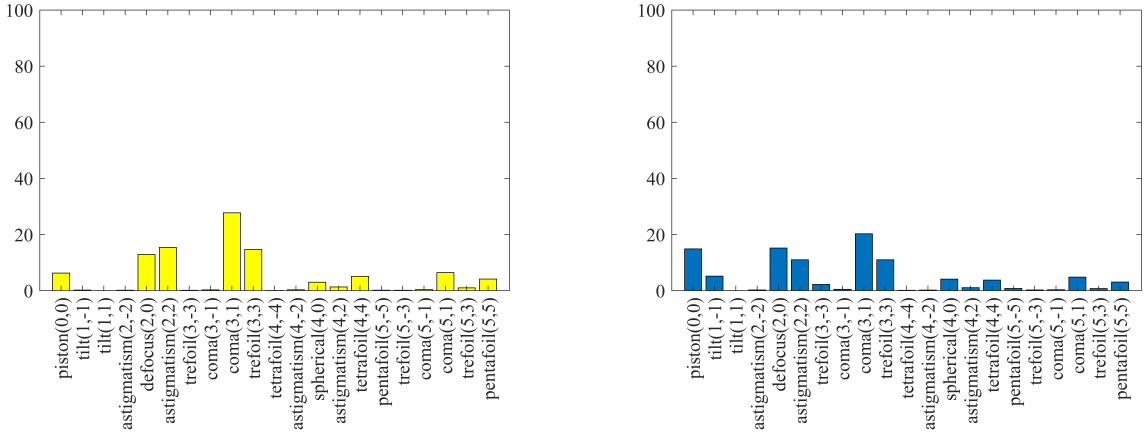

Figure 11. Aberrations weight expressed in %, estimated at elevation angle equal to 60°. The left histogram refers to the case in which only gravitational load in applied; the right histogram refers to the case in which both gravitational load and thermal load to the x_+ side of the BUS are applied.

As an example, in Fig. 11 the result of the analysis of one of the scenarios described above by the Zernike polynomial representation is shown. The histograms in Fig. 11 show the optical aberrations versus their percentage weight related to two SRT main reflector deformation maps simulated by FE at 60°. Panel on the left shows the optical aberrations which characterize the deformation map resulting when only gravitational loads are applied to the whole BUS. Instead, panel on the right shows the optical aberrations resulting when thermal loads of 5°C are applied to right half of the BUS in addition to the gravitational ones. The comparison between the two panels in Fig. 11 confirms that the surface deformations due to gravitational loads applied to the BUS results greater than those resulting from thermal loads. However, it is worth to note that the Zernike polynomial representation allows to highlight that in the 60° FE scenario defocus (2,0), astigmatism (2,2), coma (3,1) and trefoil (3.3) are the main optical aberrations that gravitational loads cause on the SRT main reflector. When aberrations due to thermal loads are added result in a slight compensation of astigmatism (2,2), coma (3,1) and trefoil (3, 3). On the contrary, piston (0,0), tilt (1,-1) defocus (2,0) and trefoil (3,-3) result slightly increased.

5. CONCLUSIONS

This paper is devoted to the the study of the effects produced by environmental thermal loads due to solar radiation on the performances of the Sardinia Radio Telescope.

First, the impact on pointing was studied. A sensitivity analysis made possible to establish which are the parts of the antenna producing the greatest pointing errors, when thermally stressed. The sensitivity analysis showed that the component that needs to be monitored most carefully is the alidade. The numerical method for estimating the temperature generated by solar radiation was calibrated using experimental data from thermographic surveys. This made it possible to simulate simplified and realistic thermal scenarios taking into account not only radiation but also convection and shading phenomena.

The simulated temperature sets were applied to the Finite Element model for the calculation of pointing errors. The computational power available allows the structural response to be simulated in a few seconds despite the complexity of the model. Hence, it will be possible to use the FEM in a loop scheme for real-time error correction.

Only the results in terms of elevation and azimuth angle variation for the most critical component, the alidade, were presented. The results of the Finite Element analysis show that among the simulated thermal scenarios, the highest value of azimuth angle change is about 11 arcsec when the antenna is set at 80°elevation angle and facing east in November; otherwise, the greatest elevation angle variation (about 8 arcsec) is achieved in August with 30° elevation angle and south orientation, see Fig. 5. Moreover, no seasonal trend has been identified. Since, under different conditions of elevation and orientation, pointing errors were found greater in fall month than in summer, it is not possible to relate the phenomenon to the value of the average environmental temperature. Rather, the real cause is to be found in the distribution of temperatures among all the trusses of the alidade, focusing on the thermal gradients between the elements in symmetrical positions with respect to the plane of symmetry. It is therefore evident that the differentiated exposure of the structural elements to sunlight plays a crucial role.

Second, it was then investigated how thermal loads produced by solar radiation can warp the shape of the main mirror surface adding large scale deformations which result in a loss of surface accuracy and, eventually, in an antenna performance loss. The temperature gradients in the BUS revealed by the thermographic surveys were used to assume simplified scenarios for analysing the phenomenon. Different configuration of temperature gradients were analysed using the finite element method. When comparing the maps in Figs. 7-10, it is evident that the gravitational load produces more important effects than the thermal one. The aspect is also visible when comparing the rms values in Tabs. 1, 2 and 3 . However, it is clear that the contribution given by the temperature distribution is enough to modify the deformation of the dish surface resulting from only the gravitational load. This leads to consider that it is effective to take into account the thermal effects in the antenna control scheme, in order to mitigate the surface errors. Therefore, although BUS heating has insignificant effects on SRT performance in terms of pointing error, it is important to evaluate its influence on aperture efficiency.

Furthermore, the effect of thermal gradients on the sub-reflector was not considered in this work. Although the subreflector is expected to affect pointing less than the alidade does, its contribution is worth analyzing in a forthcoming study.

Concluding, this study reveals the need to continuously monitor the temperature of the structural elements of the entire radio telescope. This can be done placing thermal sensors conveniently distributed on the antenna elements which the FEM analysis showed to be much more sensitive to the thermal loads. Besides, it is desirable that the metrological system consists of sensors capable of measuring both causes and effects. In this way, not only it is possible to process the acquired data for the errors estimation by the FE method, but also to compare the simulated structural behavior with that the real radiotelescope in order to update the FE model.

Acknowledgements
The Enhancement of the Sardinia Radio Telescope (SRT) for the study of the Universe at high radio frequencies is financially supported by the National Operative Program (Programma Operativo Nazionale - PON) of the Italian Ministry of University and Research "Research and Innovation 2014-2020", Notice D.D. 424 of 28/02/2018

for the granting of funding aimed at strengthening research infrastructures, in implementation of the Action II.1 - Project Proposals PIR01_00010 and CIR01_00010.

REFERENCES

[1] Govoni, F., Bolli, P., Buffa, F., Caito, L., Carretti, E., Comoretto, G., Fierro, D., Melis, A., Murgia, M., Navarrini, A., et al., "The high-frequency upgrade of the sardinia radio telescope," in [*2021 XXXIVth General Assembly and Scientific Symposium of the International Union of Radio Science (URSI GASS)*], 1–4, IEEE.

[2] Baars, J. W., [*The paraboloidal reflector antenna in radio astronomy and communication*], vol. 348, Springer (2007).

[3] Baars, J. W. and Kärcher, H. J., "Seventy years of radio telescope design and construction," *URSI Radio Science Bulletin* **2017**(362), 15–38 (2017).

[4] Baars, J. W. and Kärcher, H. J., [*Radio Telescope Reflectors*], vol. 447, Springer (2018).

[5] Fu, L., Ling, Q. B., Geng, X. G., Wang, J. Q., Jiang, Y. B., Lin, F. Y., and Zhang, Y. F., "The alidade temperature behaviour of tm65m antenna and its effects on pointing accuracy," in [*Advances in Optical and Mechanical Technologies for Telescopes and Instrumentation II*], **9912**, 99124J, International Society for Optics and Photonics (2016).

[6] Ambrosini, R., Grueff, G., Morsiani, M., Maccaferri, G., Zacchiroli, P., and Orfei, A., "Analysis of the alidade temperature behaviour of the medicina vlbi radiotelescope," *Astrophysics and Space Science* **239**(2), 247–258 (1996).

[7] Pisanu, T., Buffa, F., Poppi, S., Marongiu, P., Serra, G., Vargiu, G. P., and Concu, R., "The srt inclinometer for monitoring the rail and the thermal gradient effects on the alidade structure," in [*Ground-based and Airborne Telescopes V*], **9145**, 91454R, International Society for Optics and Photonics (2014).

[8] Ukita, N., Ezawa, H., Ikenoue, B., and Saito, M., "Thermal and wind effects on the azimuth axis tilt of the aste 10-m antenna," *Publ. Natl. Astron. Obs. Japan* **10**, 25–33 (2007).

[9] Zhao, Y., Du, J., Xu, Q., and Bao, H., "Real-time monitoring of the position and orientation of a radio telescope sub-reflector with fiber bragg grating sensors," *Sensors* **19**(3), 619 (2019).

[10] Greve, A., Bremer, M., Penalver, J., Raffin, P., and Morris, D., "Improvement of the iram 30-m telescope from temperature measurements and finite-element calculations," *IEEE transactions on antennas and propagation* **53**(2), 851–860 (2005).

[11] Stochino, F., Cazzani, A., Poppi, S., and Turco, E., "Sardinia radio telescope finite element model updating by means of photogrammetric measurements," *Mathematics and Mechanics of Solids* **22**(4), 885–901 (2017).

[12] Buffa, F., Pinna, A., and Sanna, G., "A simulation tool assisting the design of a close range photogrammetry system for the sardinia radio telescope," (2016).

[13] Buffa, F., Causin, A., Cazzani, A., Poppi, S., Sanna, G., Solci, M., Stochino, F., and Turco, E., "The sardinia radio telescope: a comparison between close-range photogrammetry and finite element models," *Mathematics and Mechanics of Solids* **22**(5), 1005–1026 (2017).

[14] Greve, A. and Karcher, H. J., "Performance improvement of a flexible telescope through metrology and active control," *Proceedings of the IEEE* **97**(8), 1412–1420 (2009).

[15] Bolli, P., Orlati, A., Stringhetti, L., Orfei, A., Righini, S., Ambrosini, R., Bartolini, M., Bortolotti, C., Buffa, F., Buttu, M., et al., "Sardinia radio telescope: General description, technical commissioning and first light," *Journal of Astronomical Instrumentation* **4**(03n04), 1550008 (2015).

[16] Gawronski, W., "Three models of wind-gust disturbances for the analysis of antenna pointing accuracy," *IPN progress report* **42**(149) (2002).

[17] White, E., Ghigo, F., Prestage, R., Frayer, D., Maddalena, R., Brandt, J., Egan, D., Nelson, J., Ray, J., et al., "Green bank telescope: Overview and analysis of metrology systems and pointing performance," *Astronomy & Astrophysics* **659**, A113 (2022).

[18] Attoli, A., Stochino, F., Buffa, F., Poppi, S., Serra, G., Sanna, G., and Cazzani, A., "Sardinia radio telescope structural behavior under solar thermal load," *Structures* **39**, 901–916 (2022).

[19] Khemlani, L., "Autodesk revit: implementation in practice," *White paper, Autodesk* (2004).

[20] Prado, R. T. A. and Ferreira, F. L., "Measurement of albedo and analysis of its influence the surface temperature of building roof materials," *Energy and Buildings* **37**(4), 295–300 (2005).
[21] Kosky, P., Balmer, R., Keat, W., and Wise, G., "Exploring engineering," (2013).
[22] Nikolic, B., Prestage, R., Balser, D., Chandler, C., and Hills, R., "Out-of-focus holography at the green bank telescope," *Astronomy & Astrophysics* **465**(2), 685–693 (2007).
[23] Hunter, T. R., Schwab, F. R., White, S. D., Ford, J. M., Ghigo, F. D., Maddalena, R. J., Mason, B. S., Nelson, J. D., Prestage, R. M., Ray, J., et al., "Holographic measurement and improvement of the green bank telescope surface," *Publications of the Astronomical Society of the Pacific* **123**(907), 1087 (2011).
[24] Wang, J. and Silva, D. E., "Wave-front interpretation with zernike polynomials," *Applied optics* **19**(9), 1510–1518 (1980).
[25] Buffa, F., Serra, G., and Poppi, S., "Hop user guide," tech. rep., OAC-Internal Report (2018).